# Conversion of Colloidal ZnO–WO3 Heteroaggregates into Strongly Blue Luminescing ZnWO4 Xerogels and Films

**ARTICLE** *in* CHEMISTRY OF MATERIALS · JANUARY 1998

Impact Factor: 8.35 · DOI: 10.1021/cm9704591



**5 AUTHORS**, INCLUDING:

Lubomir Spanhel
Université de Rennes 1
**55** PUBLICATIONS **3,540** CITATIONS

SEE PROFILE

# Conversion of Colloidal $ZnO-WO_3$ Heteroaggregates into Strongly Blue Luminescing $ZnWO_4$ Xerogels and Films

M. Bonanni, L. Spanhel,* M. Lerch, E. Füglein, and G. Müller

*Bayerische Julius-Maximilians-Universität Würzburg, Lehrstuhl für Silicatchemie Röntgenring 10, D-97070 Würzburg, Germany*

F. Jermann

*Siemens AG Corporate Technology, Otto-Hahn-Ring 6, D-81730 Munich, Germany*

*Received June 30, 1997. Revised Manuscript Received October 7, 1997*[⊗]

The colloidal synthesis of $ZnO-WO_3$ heteroaggregates composed of 3−5 nm particles is presented. These sols can be used to prepare nanocrystalline $ZnWO_4$ xerogels, powders, and thin films with strong blue fluorescence (quantum yield between 25 and 50% at room temperature). The conversion of the precursor aggregates into nano- and microcrystalline monoclinic $ZnWO_4$ Sanmartinite has been followed by XRD, DTA−TG−MS, SEM, FTIR, optical absorption, and fluorescence methods. The $ZnWO_4$ crystallites start to develop at 350 °C, and their mean crystal size increases with temperature to 35 nm at 400 °C and 120 nm at 600 °C. At the same time, the fluorescence intensity increases by 3 orders of magnitude within the aforementioned temperature regime, no matter whether X-rays or UV photons are used to excite the samples. In complementary time-resolved X-ray fluorescence investigations, two recombination processes in the micro- and millisecond range were detected. In weakly fluorescing $ZnO-WO_3$ aggregate samples at sizes between 10 and 30 nm, the slow millisecond process dominates the recombination of the charge carriers whereas in 50−275 nm crystals and above, the faster 2.5 $\mu$s process dominates the decay kinetics. Accordingly, the slow afterglow process is attributed to a recombination between electrons and holes deeply trapped at the surface of the heteroaggregates. The faster 2.5 $\mu$s recombination process takes place only in the perfectly developed Sanmartinite phase.

## Introduction

After the survey of Kröger in 1948,[1] there has been a renewed interest in $ZnWO_4$ in recent years because of possible applications as a X-ray and $\gamma$-scintillator[2,3] and laser host,[4] as well as for acoustic[5] and optical fibers.[6] $ZnWO_4$ is a nonhygroscopic, nontoxic, and self-activating luminophor exhibiting a broad, intrinsic blue emission band between 460 and 490 nm. Its scintillation properties have been studied using different excitation methods such as $^{137}Cs$ $\gamma$-rays, X-rays, and UV light.[2,4,7]

Until now $ZnWO_4$ was synthesized utilizing sintering techniques of ZnO or $ZnCO_3$ and $WO_3$ powders.[8] Alternatively, zinc and tungstate salts were precipitated from aqueous solutions and annealed above 450 °C to form $ZnWO_4$ powders.[9]

In this paper, we describe a sol−gel synthesis of $ZnWO_4$ nanocrystals of different sizes employing base-catalyzed hydrolysis and condensation of zinc and tungsten alkoxides in an alcoholic medium. The method presented offers the possibility to produce transparent blue fluorescing $ZnWO_4$ coatings, not available by conventional fabrication.

## Experimental Section

**Synthesis.** The preparation of $ZnWO_4$ xerogels and films took place according to the flowchart shown in Figure 1.

Zinc acetate [$Zn(OAc)_2 \cdot 2H_2O$ from Fluka] was dehydrated with acetic anhydride (from Grüssing), yielding $Zn_4O(OAc)_6$ clusters.[10] In the next step, 600 mL of a 0.1 M dehydrated powder suspension in absolute ethanol (Rotipuran) was refluxed at 80 °C over a period of ∼180 min. The resulting Zn precursor was identified as $[Zn_{10}O_4(OAc)_{12}](H_2O)(EtOH)_7$ derived from chemical elementary analysis, MS, XRD, FTIR, $^1H$ NMR, and $^{13}C$ NMR spectra, indicating the presence of tetrahedral cluster species.

A 600 mL suspension of 0.1 M tungsten hexamethanolate (from H. C. Starck) in ethanol was refluxed at 100 °C under ambient laboratory conditions, yielding clear $WO_3$ cluster

* Corresponding author. E-mail: spanhel@silchem.uni-wuerzburg.de.
⊗ Abstract published in *Advance ACS Abstracts,* November 15, 1997.

(1) Kröger, F. A. *Some aspects of the luminescence of solids*; Elsevier: Amsterdam, 1948.
(2) Blasse, G.; Grabmaier, B. C. *Luminescent Materials*; Springer-Verlag: Berlin, 1994.
(3) Grassmann, H.; Moser, H.-G.; Lorenz, E. *J. Lumin.* **1985**, *33*, 109.
(4) Kolbe, W.; Petermann, K.; Huber, G. *IEEE J. Quantum Electron.* **1985**, *QE-21*, 1596.
(5) Pisarevskii, Y. V.; Silvestrova, I. M.; Voszka, R.; Peter, A.; Földvari, I.; Janszky, J. *Phys. Status Solidi A* **1988**, *107*, 161.
(6) Rushbrooke, J. G.; Ansorge, R. E. *Nucl. Instrum. Methods Phys. Res. A* **1989**, *280*, 83.
(7) Ovechkin, A. E.; Ryzhikov, V. D.; Tamulaitis, G.; Zukauskas, A. *Phys. Status Solidi A* **1987**, *103*, 285.
(8) Jander, W.; Wenzel, W. *Z. Anorg. Allg. Chem.* **1941**, *246*, 67.
(9) Lesne, J. P.; Caillet, P. *Can. J. Spectrosc.* **1973**, *18*, 69.
(10) Greenwood, N. N.; Earnshaw, A. *Chemie der Elemente*; VCH-Verlag: Weinheim, 1990; p 1557.

S0897-4756(97)00459-6 CCC: $15.00 
Published on Web 01/19/1998

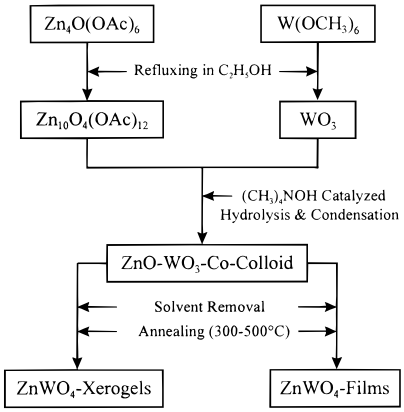


**Figure 1.** Flowchart for the preparation of $ZnWO_4$ xerogels and films.

solutions as detected in the optical absorption spectra (see Results and Discussion).

Subsequently, both cluster solutions were mixed (Zn:W = 1) and reacted with a 2.2 M methanolic tetramethylammonium hydroxide solution (TMAH from Alfa, Zn:TMAH = 1:5). The produced co-condensed colorless 0.05 M $ZnO-WO_3$ sol was optionally concentrated on a rotary evaporator ($10^{-2}$ bar, 40 °C) in order to provide coating solutions for film preparations. Alternatively, complete removal of the solvent resulted in yellowish colored gels which have been subsequently annealed under vacuum at 250 °C. Finally, the xerogels were sintered under air flow at temperatures between 300 and 800 °C for 5 h to produce nano- and microcrystals of $ZnWO_4$.

**Optical Characterization.** Optical absorption spectra of the colloidal solutions were recorded with a Hitachi U 3000 spectrometer using 0.1 mm quartz cells. Quartz slides as substrates were used to record the optical absorption spectra of the films. Photoluminescence emission and excitation spectra were detected with a Perkin-Elmer LS 50B spectrofluorimeter. All fluorescence excitation spectra were corrected for the varying intensity with wavelength of the excitation lamp. Front face accessories and 2 mm quartz cells were used. The fluorescence quantum yield $Q_{fl}$ of the $ZnWO_4$ xerogel powders was determined at room temperature, employing 254 nm excitation source of a Zeiss-PMQ 3 spectrophotometer and commercial blue fluorescing strontium halophosphate ($Sr_5(PO_4)_3(F,Cl):Sb^{3+}$) as a fluorescence standard ($Q_{fl} = 0.65$).

**X-ray Diffraction.** X-ray diffraction measurements on gel powders were performed with a Cu $K\alpha_1$ STOE STADIP system using Bragg−Brentano reflection geometry.

**Thermal Analysis.** The differential thermal analytic (DTA) and thermogravimetric (TG) data were collected with a Setaram TAG 24 thermoanalyzer connected to a quadropole mass spectrometer QMG 511. The samples were heated in oxygen stream at 2 K $min^{-1}$ against burned kaolin as reference (thermally stable up to 1500 °C).

**FTIR Measurements.** The FTIR transmission spectra were recorded with a Nicolet Magma 750 spectrometer using KBr pellets.

**X-ray Fluorescence.** Steady-state and time-resolved scintillation studies were performed on an apparatus equipped with a 50 kV tungsten X-ray source (run at 40 mA) and a photomultiplier. For the time-resolved measurements, samples were exposed to ~0.5 ms X-ray pulses utilizing single-photon counting. The decay time of the X-ray source was 20 $\mu$s.

## Results and Discussion

**Structural Characterization.** Figure 2 shows changes in the X-ray diffraction patterns of the co-condensed $ZnO-WO_3$ xerogels and of the $ZnWO_4$ nanocrystals heated in air at different temperatures. The reference diagrams of monoclinic $ZnWO_4$, hexagonal

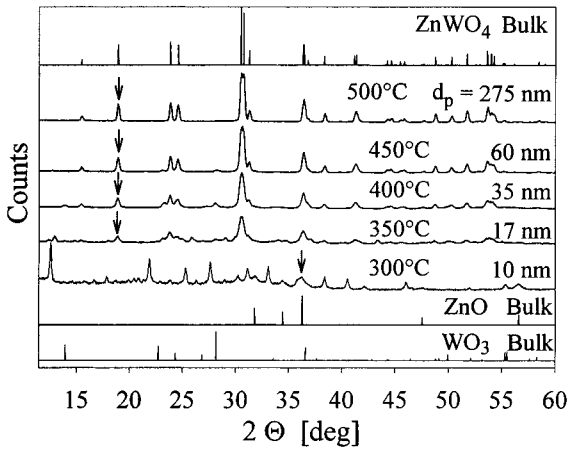


**Figure 2.** X-ray diffraction patterns of the $ZnO-WO_3$ xerogel powder and of differently sized $ZnWO_4$ nanocrystals produced after thermal annealing. JCPDS reference data of the monoclinic $ZnWO_4$ (Sanmartinite), hexagonal ZnO (Wurtzite) and hexagonal $WO_3$ are also included. Marked reflections were used for determination of the crystal size.

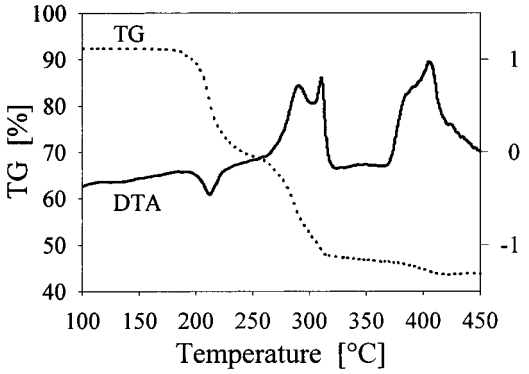


**Figure 3.** Results of the thermal analysis (DTA-TG). The sample was heated at 2 K $min^{-1}$ from 100 to 450 °C under oxygen flow.

ZnO and $WO_3$[11a−c] along with average crystal sizes (determined with the program package VISUAL $X^{POW}$) are also included. Up to 300 °C, the XRD patterns of the $ZnO-WO_3$ xerogel show the characteristic reflections of the ZnO Wurtzite nanocrystals and additional reflections indicating another phase which cannot be identified at present. Furthermore, at 350 °C, characteristic $WO_3$ and $ZnWO_4$ reflections appear in the diagram. The nanocrystal aggregates grow further with increasing annealing temperature, approaching sizes around 275 nm at 500 °C in gel powders and around 100 nm in films, respectively. Above 450 °C, the $WO_3$ reflections are no longer detected in XRD diagram indicating a completed conversion of the heteroaggregates into the pure $ZnWO_4$ Sanmartinite phase.

Figure 3 shows the differential thermal analysis (DTA) and thermogravimetry (TG) data collected on $ZnO-WO_3$ xerogels preheated at 100 °C under vacuum overnight and at 100 °C in air for 60 h. The DTA−TG experiment was performed in oxygen stream. The corresponding reaction products simultaneously detected in a mass spectrometer and the attributed events are listed in Table 1.

The results indicate several processes taking place prior to and during the development of the $ZnWO_4$

(11) (a) JCPDS 15-0774. (b) Ibid. 36-1451. (c) Ibid. 33-1387.

**Table 1. Results of DTA−TG−MS Measurement**

| temp range (°C) | weight loss (%) | MS products | reaction products and events |
|---|---|---|---|
| 200−210 | 21 | $H_2O$, CO, $CO_2$, $(CH_3)_4N$ | $(CH_3)_4NOH$ and weakly bonded acetate |
| 270−290 | 17 | $H_2O$, CO, $CO_2$ | loss of bidentate acetate ligands |
| 290−310 | 4 | $H_2O$, CO, $CO_2$ | loss of bidentate acetate and water |
| 370−400 | 2 | | primary crystallization to $ZnWO_4$ and $WO_3$ |
| 400−415 | 1 | | secondary crystallization to $ZnWO_4$ and $WO_3$ |

phase. The first endothermic process between 200 and 250 °C produces a significant loss in mass accounting for about 25% of the initial weight. During this firing step, tetramethylammonium hydroxide, water, and weakly bonded acetate ligands are liberated. The next exothermic step starting around 280 °C produces a further loss in mass of about 20%. This corresponds to the removal of strongly bonded bidentate acetate ligands which coincides with observations made by Sakohara et al. on acetate-capped ZnO nanocrystals[12] and our own FTIR experiments presented below. Additionally, this second step liberates water molecules around 300 °C.

The next exothermic process seen between 370 and 415 °C represents the crystallization of $ZnWO_4$ and $WO_3$ nanocrystals which ends at temperatures between 450 and 500 °C (without major mass losses), accompanied by the disappearance of the $WO_3$ phase (see XRD in Figure 2) and by further water removal.

The liberation of water above 350 °C was not detected in the mass spectrometer, but it has been proved in TG and additional FTIR investigations. The result of this complementary FTIR study performed on annealed samples is depicted in Figure 4. At 200 °C, the IR spectrum of the $ZnO-WO_3$ xerogels indicated the presence of bridging and bidentate carboxylate ligands represented by three absorption bands located at 1404 $cm^{-1}$ (symmetrical C−O stretching vibration for both types of ligands), at 1487 $cm^{-1}$ (C═O stretching vibration in bidentate), and at 1570 $cm^{-1}$ (C═O stretching vibration in bridging ligands). With an increase in temperature up to 250 °C, the IR absorption bands of the bridged ligands become almost completely suppressed whereas the bidentate ligands reside at the ZnO surface up to 300 °C. Above 300 °C, the bidentate ligand absorption at 1487 $cm^{-1}$ is no more detected in the IR spectrum in agreement with the above presented DTA−TG−MS data.

Additionally, the IR spectra show how the absorption bands of OH groups (stretching vibration at 3450 $cm^{-1}$) and water molecules (deformation vibration at 1640 $cm^{-1}$) change during the thermal condensation. One recognizes that the main amount of OH groups and water molecules is liberated between 200 and 400 °C. The degree of hydroxylation gradually decreases at higher temperatures and around 800 °C (not shown in Figure 4), the OH and water absorption bands are no more detected in the IR spectrum. Figure 4 also proves the presence of $ZnWO_4$ (lattice vibration bands between 400 and 900 $cm^{-1}$), in agreement with published data.[9]

Finally, Figure 5 displays the SEM images of differently sized $ZnWO_4$ crystals in xerogel powders (part a) and in a 500 nm thick film deposited on a quartz slide (part b). Prior to $ZnWO_4$ formation (below 300 °C), the

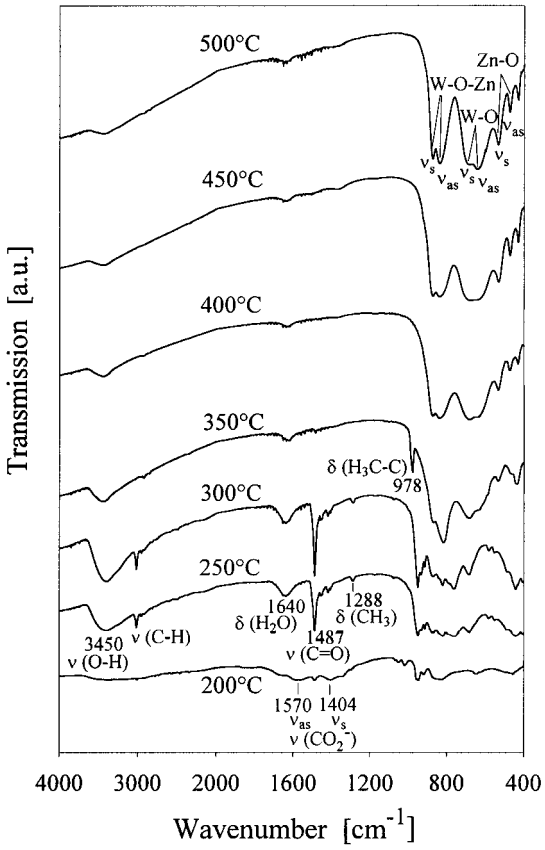


**Figure 4.** FTIR spectra of $ZnWO_4$ xerogels fired in air at various temperatures for 5 h.

$ZnO-WO_3$ xerogels are spongy whereas above 400 °C, increasingly grainy textures and faceted crystals can be seen. At 900 °C, 15 $\mu$m crystals could be produced. By comparing films and xerogel powders sintered at the same temperature, we noticed a smaller crystal size in the case of films. For example, annealing at 600 °C produces 120 nm big crystalline aggregates compared to 1 $\mu$m observed in xerogel powders. However, more detailed future HRTEM investigations will be needed to explore the internal morphology of the crystalline aggregates down to the primary particle size.

**Optical Absorption.** Figure 6a shows the optical absorption spectra of $Zn_{10}O_4(OAc)_{12}$ and $WO_3$ cluster solutions before and after mixing and subsequent reaction with tetramethylammonium hydroxide (see also the Experimental Section). For comparison, the spectrum of 3.5 nm ZnO particles synthesized in the absence of tungsten oxide is also included. In contrast to ZnO and $WO_3$ bulk crystals known to exhibit a comparable optical absorption edge located at 400 nm,[13] the strongly blue shifted spectra of the above nanocolloids (below 370 nm) reflect the presence of more or less size-quantized

(12) Sakohara, S.; Tickanen, L. D.; Anderson, M. A. *J. Phys. Chem.* **1992**, *96*, 11086.

(13) Gerischer, H. *Top. Appl. Phys.* **1979**, *31*, 115.

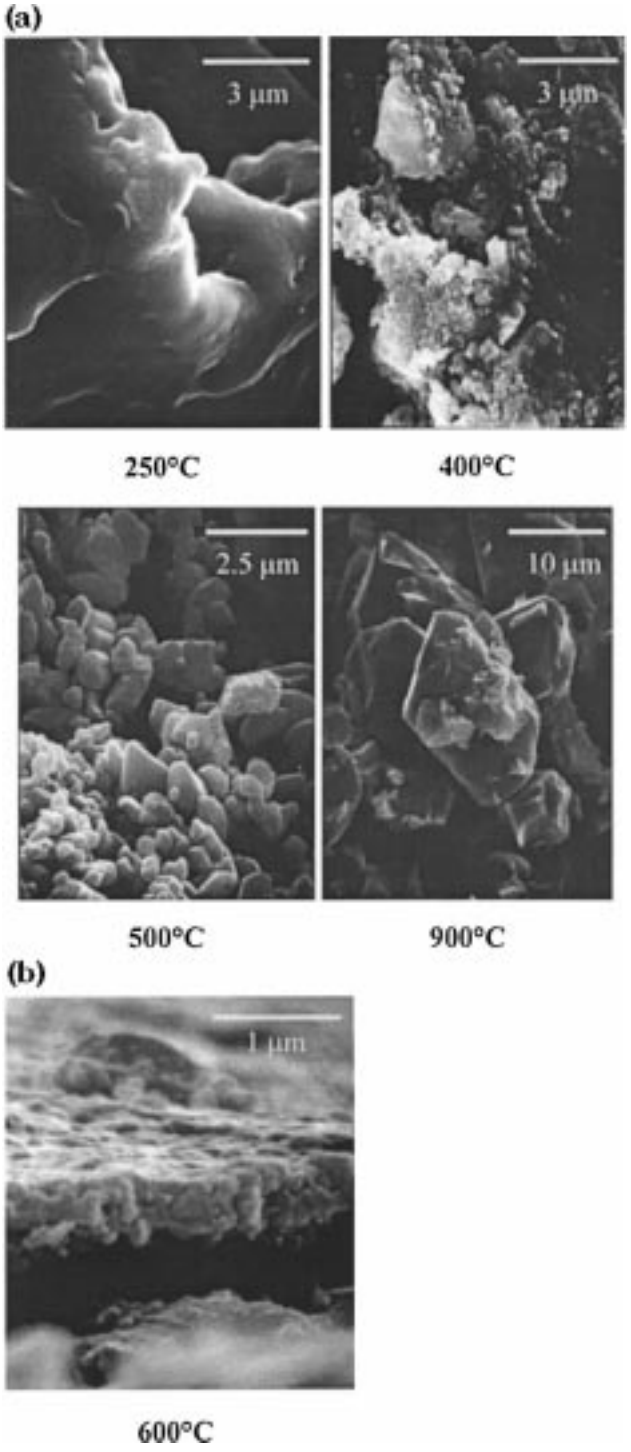


**Figure 5.** (a) Scanning electron micrographs of differently sintered $ZnWO_4$ xerogel powders. (b) Front view of a $ZnWO_4$ film on quartz glass sintered at 600 °C.

particles. Their sizes, determined in earlier transmission electron microscopy and XRD studies,[14,15] are of about 3−5 nm.

As stated in the Experimental Section, the condensed $ZnO-WO_3$ cluster solutions can be used for the preparation of transparent $ZnWO_4$ films on quartz glass slides. This made it possible to investigate changes in the optical absorption properties during thermal conversion of the consolidated $ZnO-WO_3$ nanostructures into the Sanmartinite phase. Figure 6b illustrates how the $ZnO-WO_3$ optical absorption spectrum changed with increasing sintering temperature. Between 300 and 400 °C, after the film sample lost nearly all organic surface bonded molecules, a significant blue shift of the optical absorption edge initially located at 350 nm takes place. Additionally, a shoulder at 340 nm can be observed in the optical spectrum. Above 400 °C, the spectrum starts to shift to the red with increasing temperature, and at 500 °C, the film spectra exhibit two shoulders at 270 and 350 nm. These results, in accordance to XRD observations, indicate that nanocrystalline Sanmartinite particles are produced (blue-shift), aggregating with increasing temperature to give larger nanocrystals (red-shift). This thermal conversion concomitantly activates a strong blue fluorescence which will be described in more detail in the next chapter.

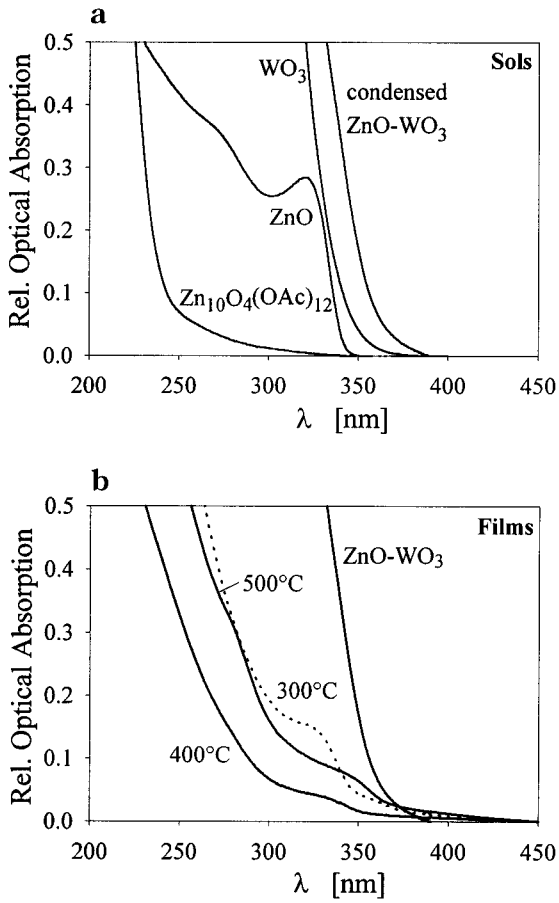


**Figure 6.** (a) Optical absorption spectra of ethanolic $Zn_{10}O_4(OAc)_{12}$ and $WO_3$ precursor cluster solutions and the resulting $ZnO-WO_3$ spectrum after hydrolysis and condensation. For comparison, the spectrum of an ethanolic ZnO colloid is also included. (b) Optical absorption spectrum of an unfired wet $ZnO-WO_3$ film before and after sintering at 300, 400, and 500 °C.

**Photoluminescence and X-ray Luminescence.** The photoluminescence excitation and emission spectra of the ZnO and $ZnO-WO_3$ nanocolloids are shown in Figure 7 ($WO_3$ colloids were found to exhibit no fluorescence). The emission spectrum showing a characteristic green-yellow fluorescence band of ZnO particles is independent of the excitation wavelength. The corresponding excitation spectrum exhibits two transitions at 275 and 325 nm, also recognized in the optical

(14) Spanhel, L; Anderson, M. A. *J. Am. Chem. Soc.* **1991**, *113*, 2826.
(15) Bedja, I.; Hotchandani, S.; Kamat, P. V. *J. Phys. Chem.* **1993**, *97*, 11064.

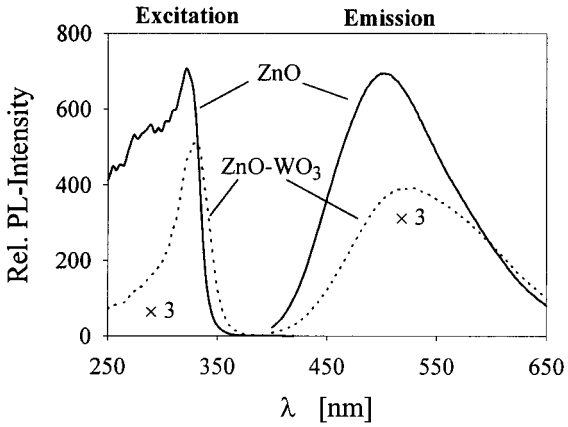


**Figure 7.** Photoluminescence excitation ($\lambda_{em}$ = 520 nm) and emission spectra ($\lambda_{ex}$ = 330 nm) of 0.05 M ZnO− (solid line) and 0.05 M ZnO−$WO_3$ colloid (dotted line).

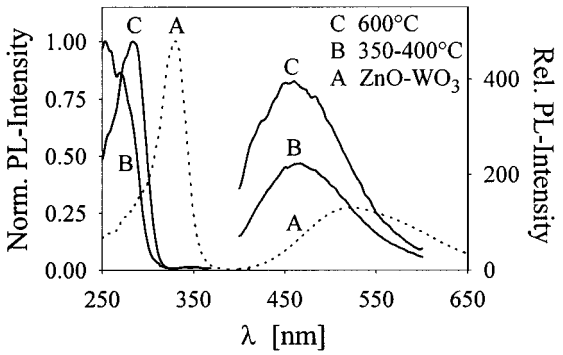


**Figure 8.** Corrected photoluminescence excitation ($\lambda_{em}$ = 460, 520 nm) and emission spectra ($\lambda_{ex}$ = 254, 310 nm) of ZnO−$WO_3$ films before (spectrum A) and after oxidative annealing between 350 and 600 °C (spectra B and C).

absorption spectrum of ZnO in Figure 6. In co-condensed ZnO−$WO_3$ colloids, however, the slightly red shifted fluorescence band as well as the high-energy transitions in the excitation spectrum are less intense indicating quenching in coupled ZnO−$WO_3$ particles [(ZnO−$WO_3$)* → $ZnO^+ + WO_3^-$]. Such a quenching of ZnO fluorescence could be observed by mixing separately prepared ZnO and $WO_3$ colloids, too. From the literature reports it is known that the conduction band electrons in $WO_3$ have more positive potential than in ZnO.[14−17] Therefore, the observed quenching in these heteroaggregates can be attributed to an interparticle electron transfer[17] (see also Figure 11 and text below), previously reported for several other colloidal semiconductor heteroaggregates.[17]

After the first firing step taking place between 200 and 250 °C, the ZnO fluorescence in ZnO−$WO_3$ xerogels or transparent films is instantaneously suppressed. This is apparently related to the evaporation of organic surface bonded molecules producing more strongly aggregated ZnO and $WO_3$ particles, and thus, a more efficient charge carrier separation. However, at higher temperatures around 350 °C, a new blue fluorescence band starts to develop, indicating a transformation of aggregated ZnO and $WO_3$ particles into a new crystalline phase.

Figure 8 depicts the corresponding temperature dependent spectral changes accompanying the activation of blue fluorescence (broad emission band peaking at 460 nm) in increasingly heated films deposited on quartz slides. As can be seen, the excitation onset of the ZnO fluorescence, initially located at 390 nm (see spectrum A at left side and Figure 7), is strongly blue shifted to 300 nm between 350 and 400 °C (spectrum B) and shifts slightly toward red at 600 °C. This blue−red shift coincides with the above presented changes in the optical absorption spectra of the thermally annealed films (Figure 6b). Whether the minor red shift of the photoluminescence excitation onset is due to aggregation of Sanmartinite nanocrystallites or due to the disappearance of the unknown crystalline phase seen in XRD diagram of the 300 °C xerogel sample (see Figure 2) cannot be decided at present. Figure 8 also demonstrates that the maximum position of the $ZnWO_4$ fluorescence band is found at higher energy compared to nonreacted ZnO−$WO_3$ heteroaggregates. Additionally, the intensity of the blue fluorescence increases significantly with increasing sintering temperature. Its quantum yield, determined on samples heated between 600 and 800 °C, ranges between 25% and 50%.

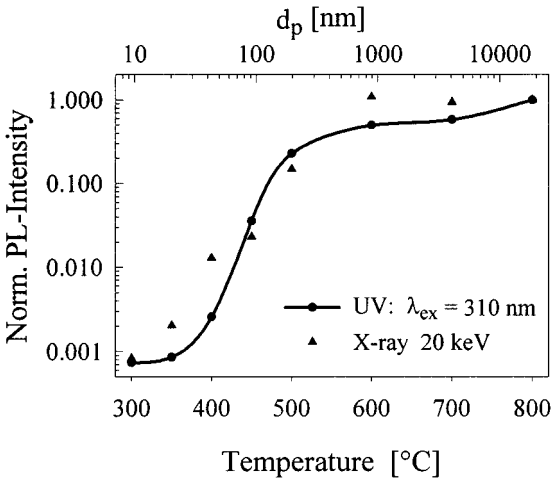


**Figure 9.** Temperature dependence of the intensity of the blue luminescence induced by UV or X-ray absorption (330 nm or 20 keV); the upper scale reflects the corresponding crystal sizes determined in XRD and SEM investigations.

In the accompanying X-ray fluorescence measurements, we detected a very similar spectral shape and temperature-dependent intensity changes of the 460 nm emission band. Figure 9 summarizes the results illustrating how the photoluminescence and X-ray fluorescence intensity changed with increasing annealing temperature and nanocrystal size. One recognizes a significant fluorescence activation between 400 and 500 °C and an intensity plateau at 600 °C, no matter whether UV or X-ray excitation were used. This figure also illustrates that above 600 °C an intensity plateau is reached. The earlier presented XRD data which proved the presence of $WO_3$ up to 450 °C suggest that the substantial increase in the PL intensity between 400 and 500 °C is caused by the completed conversion into the Sanmartinite phase.

The X-ray fluorescence decay curve obtained from time-resolved measurements under stationary conditions is shown in Figure 10, reflecting the existence of

(16) Bahnemann, D.; Bockelmann, D.; Goslich, R. *Solar Energy Materials* **1991**, *24*, 564.

(17) Kamat, P. V. *Prog. Inorg. Chem.* **1997**, *44*, 273.

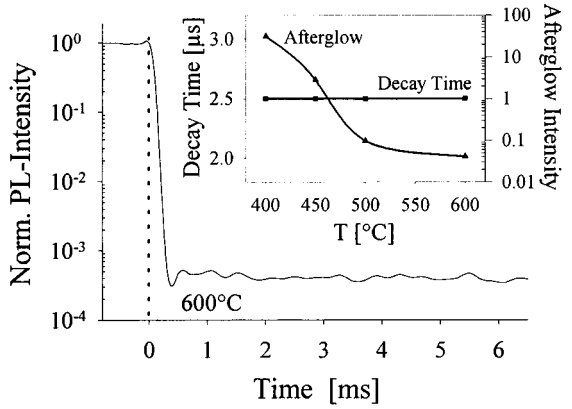


**Figure 10.** X-ray luminescence decay curve detected on a $ZnWO_4$ xerogel (fired at 600 °C) at 460 nm. Inset: Time constant of the faster recombination process as a function of the sintering temperature (left-hand side); temperature-dependent intensity of the slow afterglow process expressed in percent after 3 ms (right-hand side).

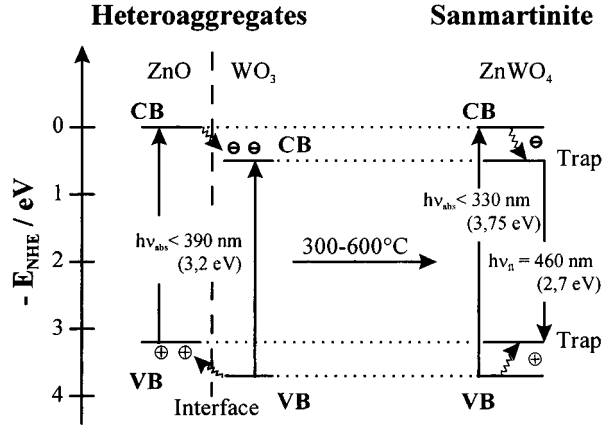


**Figure 11.** Electronic correlation diagram of the $ZnO-WO_3$ sandwich before and after the thermal conversion into $ZnWO_4$: CB = conduction band, VB = valence band, $E_g$ = bandgap.

two radiative recombination processes in $ZnWO_4$ nanocrystals. The lifetime of the first recombination process was determined to about 2.5 $\mu$s (comparable with 5 $\mu$s known for $ZnWO_4$ bulk crystals[2]) whereas the slow "afterglow" process takes several milliseconds, not resolved under our detection conditions. The intensity of the slow process (expressed in percent of the initial value after 3 ms) decreased from 30 to 0.04% within the temperature range between 400 and 600 °C, concomitant with an increase in amplitude of the faster 2.5 $\mu$s process. The lifetimes of both processes did not change with increasing temperature.

**Electronic Correlation Diagram.** The above results deserve a more detailed discussion of the excitation and emission mechanism of the blue fluorescence band, as well as of the related decay kinetics.

Figure 11 depicts energetic positions of the conduction and valence bands (CB, VB) of the $ZnO-WO_3$ heteroaggregate before and after the transformation into $ZnWO_4$ nanocrystals. ZnO and $WO_3$ in a nonquantized state have about the same bandgap energy around 3.2 eV. Hence, an absorption of UV photons (below 390 nm) produces electron−hole pairs in both components of the heteroaggregate whereas absorption of X-ray photons is more efficient in the tungsten oxide (due to substantially higher electron density). Subsequently, the photogenerated holes are trapped on the ZnO part while the electrons are accumulated on $WO_3$ which is thermodynamically allowed (see Figure 11). These spatially trapped charge carriers can react on the surface with adsorbed organic molecules, water, and oxygen, which explains the above-mentioned quenching of the ZnO fluorescence in heteroaggregate structures.

Above 300 °C, the thermal conversion begins producing blue fluorescing $ZnWO_4$ nanocrystals after the main part of chemisorbed organic molecules are removed from the aggregate surface. This suggests a new electronic diagram shown in the right part of Figure 11. Apparently, the energetic VB and CB positions of the initial sandwich are preserved in $ZnWO_4$ nanocrystals, which is reflected in the experimentally observed electronic transition at 330 nm. Upon comparison of the diagrams in Figure 11, it becomes obvious that the initial lowest edge of the CB in $WO_3$ and the upper edge of the VB in ZnO serve probably as deep trap states in $ZnWO_4$. Although we do not have a direct experimental proof of it, interestingly, the energy difference between these two virtual trap levels corresponds to a wavelength of 460 nm, which coincides with the intensity maximum of the experimentally detected blue fluorescence band.

The above-presented changes in the decay kinetics can be explained as follows. During the primary and secondary crystallization events between 300 and 400 °C, only a minor part of electron−hole pairs recombine in a radiative manner. The slow millisecond recombination process contributing with 30% to this weak emission of blue light could be attributed to a tunneling of the trapped electrons toward deeply trapped (eventually spatially separated) holes within $ZnWO_4-WO_3$ aggregate nanostructures, also recognized as separate phases in the XRD diagram. The faster microsecond component, on the other hand, contributing with 70% to the weak blue emission, reflects the recombination of the charge carriers within pure Sanmartinite phase. Between 400 and 600 °C, where the blue fluorescence becomes very strong, the slow process is suppressed, due to the completed conversion into Sanmartinite eliminating increasingly the possible competing trapping of electrons on $WO_3$ and holes on OH-groups (seen also as disappearance of $WO_3$ in XRD diagram and diminishing of water and OH absorption in FTIR spectrum).

The above-proposed qualitative model based on the homogeneity and the related spatial separation of charge carriers is not the only possible explanation of our experimental observations. An alternative interpretation considering a competition of radiative interior and nonradiative interface processes in differently sized crystals might be also taken into account. Accordingly, with increasing crystal size, the radiative interior recombination processes within nanocrystals should increasingly dominate, due to decreasing surface-to-volume ratio. However, the percentage of surface molecules in $ZnWO_4$ crystallites has been calculated to decrease from only 15% for 20 nm particles to about 2% for 200 nm crystals. This drop in percentage of surface molecules hardly explains the activation of the blue fluorescence by nearly 3 orders of magnitude within this size regime. This becomes even more evident if one calculates the transit time $\tau$ of the charge carriers

toward the interface as function of nanocrystal size according to the well-known formula $\tau = D_p^2/4\pi^2 D$ ($D_p$, particle diameter; $D$, diffusion coefficient). Taking a typical $D$ value of 0.1 $cm^2/s$, it has been calculated that it takes only 1 ps for the charge carriers to reach the interface in 20 nm particles and it still takes only 100 ps in 200 nm large crystals. These transit times are by several orders of magnitude shorter than the radiative lifetime of 2.5 $\mu$s for the fast recombination process in fairly well developed $ZnWO_4$ crystallites. Accordingly, the interface processes dominate the recombination of electrons and holes by all crystal sizes under investigation. This is also supported by the fact that the fluorescence lifetime is independent of the crystal size. Hence, the achieved fluorescence activation is best understood in terms of the completed conversion of $ZnO-WO_3$ heteroaggregates into Sanmartinite, rather than in terms of the increasing crystal size.

## Conclusions

Colloidal $ZnO-WO_3$ heteroaggregates in ethanol have shown to be suitable nanocrystalline precursors for the preparation of blue fluorescing $ZnWO_4$ xerogels and films. The above structural and optical spectroscopic data allowed to set up an electronic correlation diagram explaining the activation of the blue emission during the thermal conversion of $ZnO-WO_3$ sandwich structures into the nanocrystalline $ZnWO_4$ Sanmartinite phase. Additionally, both the spectral shape and the sintering temperature profile of the fluorescence intensity were not dependent upon whether high-energy X-rays or low-energy UV photons were used for the excitation. This suggests that not the crystal size but rather the extent to which the $ZnO-WO_3$ heteroaggregates are present governs the efficiency of the blue photoluminescence. An understanding of the size dependency of the X-ray fluorescence is important in order to judge the potential of semiconductor nanocrystals for scintillation materials. In our case, to evaluate the crystal size dependence of the blue fluorescence would necessitate, first, an extraction of the ZnO and $WO_3$ phases from the already developed $ZnWO_4$ nanocrystals. Second, it would necessitate to avoid the presence of fluorescence quenchers represented by OH groups and water molecules during the $ZnWO_4$ nanocrystal growth. Consequently, an improved synthesis would be needed in future investigations. Finally, the presented work might be an aid to the synthesis new photoluminescing film materials based on thermal reaction between nanocrystallites in metal oxide heteroaggregates.

**Acknowledgment.** The authors are grateful to the Bundesministerium für Bildung und Forschung BMBF for financial support. They also thank Mr. K. Henkel from the Fraunhofer Institute for Silicate Research in Würzburg for the DTA−TG−MS measurements as well as U. Müller and Dr. F. Zwaschka from the OSRAM GmbH for the quantum yield determinations on xerogel powders. They express their gratitude to Mr. P. Tur and Mr. Dr. A. Berger for the REM measurements.

CM9704591